INJECTOR LINAC FOR SUPER-ALIS

T. Hosokawa, T. Kitayama, T. Hayasaka, S. Ido, Y. Uno,
A. Shibayama, J. Nakata, K. Nishimura and M. Nakajima.
NTT LSI Laboratories, Nippon Telegraph and Telephone Corporation,
3-1, Morinosato Wakamiya, Atsugi, Kanagawa, 243-01, JAPAN.

Abstract

An injector linac is described for Super-ALIS, the dedicated superconducting storage ring to X-ray lithography at NTT LSI Laboratories. Super-ALIS employs a low energy injection scheme. In this scheme, injection efficiency needs to be raised, since stacking is unavailable due to Super-ALIS's low injection energy levels. Strict requirements had to be met in order to improve the efficiency of the injector: large current, low transverse emittance and a narrow energy spread. A low emittance electron gun, double pre-bunchers, standing-wave accelerator cavities and an ECS were used in the injector to fulfill those requirements. The characteristics of the system are summarized below. Acceleration frequency is 2856.65 MHz. Beam energy and current are 15 MeV and 270mA, respectively. Beam energy spread is 1% (FW). Beam pulse width is 2 μs. Maximum repetition rate is 3 Hz.

Introduction

With the development of ULSI technology, applying Synchrotron Orbital Radiation (SOR) to X-ray lithography has become of major interest lately. There are several projects currently underway for developing a storage ring fully dedicated to lithography. [1]-[4] NTT LSI laboratories have also been developing lithographic storage rings, named NAR and Super-ALIS. [5], [6] NAR uses normal conducting bending magnets and adopts an energy-boost-in-the-ring scheme. It has been applied to experimental ULSI fabrication since June 1988. Super-ALIS is a compact SOR machine with superconducting bending magnets. It also uses an energy-boost-in-the-ring scheme. Its injection energy is around 15 MeV, and final energy, 600 MeV. Super-ALIS has already succeeded in beam acceleration and storage at the final energy.

Compactness and low cost are a requisite for industrial use. For these purposes, low energy injection and energy-boost-in-the-ring schemes are promising. When electron energy decreases, however, damping time becomes long but beam lifetime short, thus making commonly used stacking injection methods difficult. Therefore in this scheme, desired beam current must be injected by only one electron beam pulse. Efficient large current injection thus becomes a key technology to achieve a low energy injection scheme. For efficient injection, low transverse emittance, large current, and narrow energy spread are demanded of an injection accelerator.

We have developed an injection linac, which satisfies the above demands, for NAR and Super-ALIS. This paper describes the outline and the performance of the machine.

General Description of the linac

Figure 1. shows a block diagram of the linac system. The linac system consists of an acceleration section, an energy compression system (ECS), an energy analyzer section, an RF system, a beam monitoring system, and a control system. The control system is located in the control room, 90 m away from the main system. The other systems, including the cooling utility, are concentrated in the one place. Electrons, accelerated up to around 15 MeV in the acceleration section, enter the ECS, where their energy spread is reduced. Electron beam quality is analyzed in the energy analyzing section and the beam monitoring system. A transport system follows the linac. Electron beams are switched in the transport system, and guided into either NAR or Super-ALIS. The acceleration section is mounted on an aluminum base, and the ECS and the energy analyzing section, on the other bases. These are transported and aligned as a unit cell. The acceleration section is 3.4 m in length; ECS, 2.8 m; and the energy analyzing section,

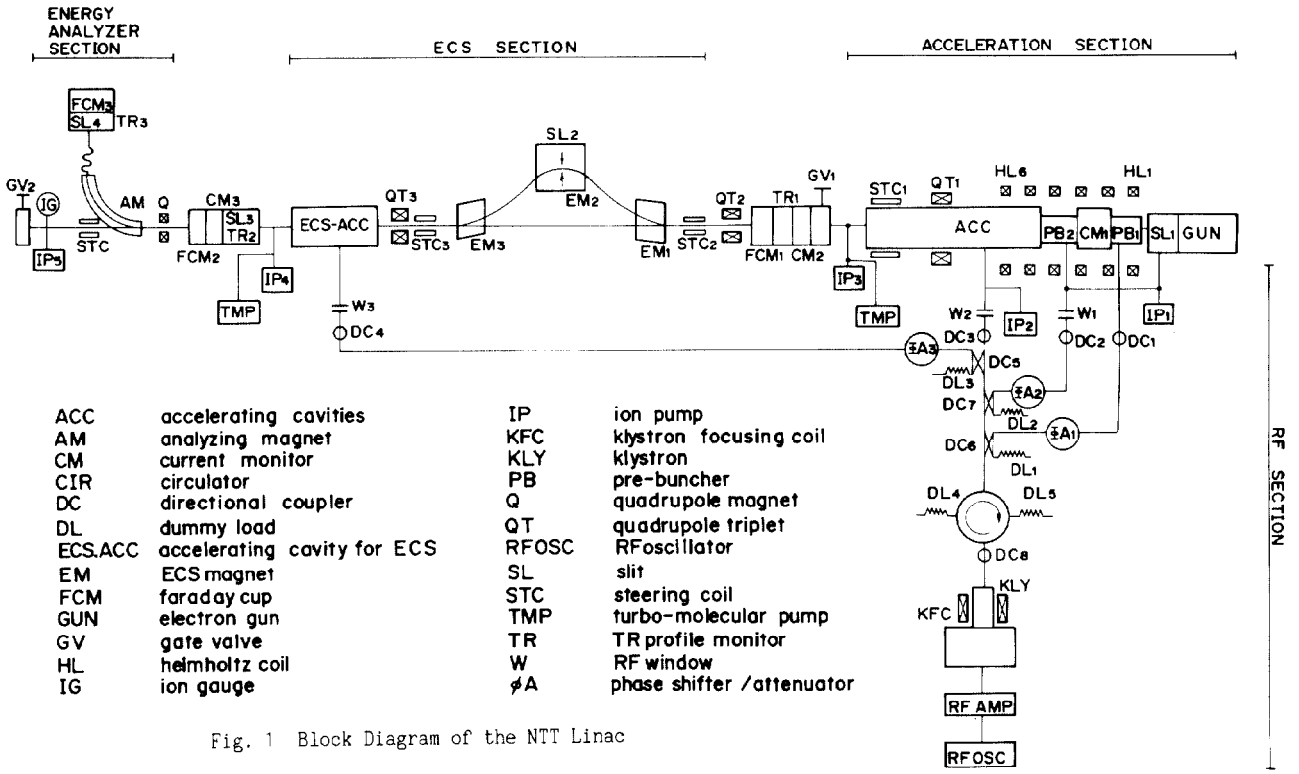

ACC	accelerating cavities	IP	ion pump
AM	analyzing magnet	KFC	klystron focusing coil
CM	current monitor	KLY	klystron
CIR	circulator	PB	pre-buncher
DC	directional coupler	Q	quadrupole magnet
DL	dummy load	QT	quadrupole triplet
ECS.ACC	accelerating cavity for ECS	RFOSC	RFoscillator
EM	ECS magnet	SL	slit
FCM	faraday cup	STC	steering coil
GUN	electron gun	TMP	turbo-molecular pump
GV	gate valve	TR	TR profile monitor
HL	helmholtz coil	W	RF window
IG	ion gauge	ϕA	phase shifter /attenuator

Fig. 1 Block Diagram of the NTT Linac

CH2669-0/89/0000-1459$01.00©1989 IEEE

Table. I . Specifications and Performance of the NTT Linac

	Specification	Performance
Beam energy	> 13 MeV	15 MeV
Beam pulse width	> 2.0 μs	2.0 μs
Beam current	> 250 mA	270 mA
Energy spread	< 1 % (FW)	1 % (FW)
Beam size	< 4.0 mmϕ	3.0 mmϕ
Beam divergence	< 0.5 mrad.	1.4 mrad.
Transverse emittance	< $1 \times 10^{-6}\pi$ m rad	$2.1 \times 10^{-6}\pi$ m rad
Repetition frequency	3 Hz max.	3 Hz max.

1.6 m. The specifications are summarized in Table I . These were determined by the injection characteristics of NAR and Super-ALIS.

Acceleration Section

The acceleration section consists of an electron gun, two pre-bunchers and the main acceleration cavities. The electron gun is a triode with an oxide cathode with a voltage of 90 kV. Electrons from the gun are velocity modulated by the bunchers as they enter the main cavities.

Characteristics of the electrons emitted from the gun affect the transverse emittance of the accelerated beams. Normalized transverse emittance is conserved in the rotationally symmetric electro-magnetic fields; [7]

$$\varepsilon_r \gamma \beta = \text{constant},$$

where ε_r, γ and β are transverse emittance, electron energy normalized by electron rest energy and electron velocity normalilzed by light velocity, respectively. Therefore the gun emittance ε_G must satisfy

$$\varepsilon_G \leq \frac{\gamma_T \beta_T}{\gamma_G \beta_G} \varepsilon_T ,$$

where ε_T is the desired emittance after acceleration. In our case, the desired emittance was $1 \times 10^{-6}\pi$ m rad. Therefore the gun emittance must be less than $4.27 \times 10^{-5}\pi$ m rad. However, as electron beams enter the acceleration cavities at various times, the normalized emittance of a group generally becomes larger during acceleration. Therefore some margins are required to the above emittance value. The measured gun emittance was $2 \times 10^{-5}\pi$ m rad, which satisfies the above condition.

Two pre-bunchers are located between the gun and the main acceleration cavities. These pre-bunchers are used for matching in the longitudinal phase space. Six solenoids are mounted around the bunchers in coaxial configuration with respect to the beam axis, supressing the divergent force effect caused by space charge.

For main accelerating cavities we have adopted a $1/2\pi$ mode standing wave type in order to achieve compactness. There are 32 cavities.

Energy Compression System

ECS consists of three magnets(EM1~EM3) and an RF cavity. The bending radius is 0.15 m. A slit (SL2) is located in the middle of EM2. The slit width is variable. A radiation shield surrounds all the magnets because electron beam loss is large in this area. The off energy function is calculated to be 0.42 m at this slit. When the three magnet coils were connected in series and excited, electron beams coming from the ECS were deflected horizontally. This undesirable effect is caused by a magnet-fringing field. In order to avoid this problem, the central magnet (EM2) and the side magnets (EM1 & EM3) were excited individualy with two separate power supplies.

Energy Analyzing Section

The energy analyzing section consists of a bending magnet (AM), a slit (SL4) and a faraday cup (FCM3). The bending radius is 0.5 m. The slit width is variable. The analyzing magnet is movable and can be set off the main beam axis. This magnet is driven by a bipolar current supply in order to initialize and degauss the magnet. After the analysis, the initialization and degaussing greatly reduce the effect on the beam injection into the two storage rings. At the entrance of the analyzing magnet, an aperture (SL3, 4 mmϕ) and a profile monitor (TR2) are located. Because electron beams spread out horizontally in the magnet, some electrons hit on and are reflected off the vacuum duct, thus entering the faraday cup, and generating an erroneous analyzing signal, thus degrading analysis accuracy. In order to prevent this, an aperture supressing reflected beam is installed.

RF Section

The main oscillator is a 2856.65 MHz synthesizer. The output power level is around 10 dBm at normal operation. The RF signal from the synthesizer is pulse mudulated. RF power is transmitted by a 90 meter coaxial cable, whose transmission loss is 8.1 dB. The transmitted RF signal is fed to a TWT amplifier (CW operation), amplified additionally by three-stage planar electrode tubes (pulse operation), and is then inputted to a klystron. The maximum output power of the klystron is 10 MW and its gain is 60 dB. Output power of the klystron is divided into 4 parts, and is fed to the pre-bunchers, main accelerating cavities and the ECS cavities through attenuators, isolators and phase shifters. RF signals are detected at various points and transmitted by coaxial cables to the control room.

Beam Monitors

Beam monitors installed are current transformers, faraday cups and beam profile monitors. They are located at each end of the sub-sections, thus simplifying the adjustment procedure and making it more precise. The current transformers are magnetically shielded. The profile monitors use transition radiation (TR). The target materials are aluminum and silicon. The merits of the TR type monitor are:

(a) accurate profile capability based on good linearity between electron beam and emitted light intensity,
(b) minimal contamination effect of the vacuum space,
(c) fast time response.

A disadvantage is a lower sensitivity than a fluorescence type, especially for low energy beams. The TR sensitivity, however, is sufficient to observe even 15 MeV electron beam profiles. The profiles are monitored by TV cameras through viewing windows. The windows are made from sapphire coated with titanium. This arrangement prevents light transmissivity degradation by coloring, and cracks caused at charge-up. The titanium coating thickness is determined by elctrical conductivity and light transmissivity. Apertures, slits and faraday cups are made from oxygen-free-cupper. The faraday cup (FCM4), the aperture (SL5, 8 mm ϕ) and the profile monitor (TR4) are also located in the beam transport system at a point 4 m away from SL3. These monitors, with other ones, are used for adjustment and transverse emittance estimation. Apertures and faraday cups, except for FCM3, can be moved on and off the beam path by remote control.

Emittance Growth

Transverse characteristics of the main cavities were analyzed using the paraxial approximation.[7] In this analysis, a measured axial electric field was used. In the paraxial approximation, the relationship between transverse phase space coordinates R_1 and R_0 at the entrance and exit of the accelerating cavities can be written as

$$R_0 = M R_1 ,$$

where M is a transform matrix. If the elements of the matrix are constant, a normalized emittance is conserved. However, in the RF fields, the matrix elements are dependent on the entrance phase and energy of an incident electron. Focusing or divergent forces exerted on electrons depend on the entrance phase and the energy. Because the phase and energy of incident beams have a finite width,

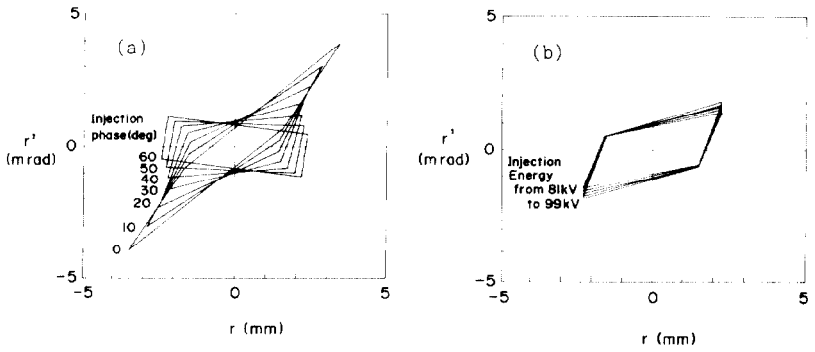

Fig. 2 Transverse emittance diagram of accelerated beams.
(a) incident beam phase : from 0 ° to 60 °
incident beam energy : 90 kV
(b) incident beam phase : 30 °
incident beam energy : 90 kV ±10%

normalized emittance of the beams generally increases in the acceleration process. Therefore it is important to estimate this increase.

Figure 2(a) displays an exit beam transverse emittance diagram, the incident beam phase shown as a parameter. An incident beam size of 4 mm, a beam divergence of ±40 mrad, and a rectangular phase diagram shape are assummed. An emittance diagram of the exit beam is made up of a set of these rectangular diagrams. From the longitudinal analysis, the optimum incident phase was calculated to be from 20° to 40° . This leads to the conclusion that the emittance increases by a factor of less than 1.5. The figure also indicates that the exit beam is divergent. This divergence can be corrected by focusing the incident beams or by using the quadrupole triplet located near the exit part of the cavities.

Figure 2(b) shows the emittance growth caused by incident beam energy spread. A spread of 90 kV±10% is assummed. Incident phase is 30° . This figure indicates that the emittance growth caused by the incident beam energy spread is small.

Experimental Performance

Figure 3. shows the beam current waveforms at several places in the linac system with the ECS in operation. Gun emission current is 520 mA and the accelerated beam current is 320 mA, thus the transmissivity of the accelerating cavities is 62%. Figure 3 (d) shows the waveform through the energy analyzer. Energy aperture width was 1%, and the beam current within a 1% energy spread (FW) was 270 mA.

Figure 4 shows the energy spectrum. The energy spread was 0.94% (FWHM). The sub-peak signal appearing in the figure is partly caused by the error signal mentioned above.

Figure 5 shows the beam profile at the exit of ECS (TR2). Beam diameter is 3 mm. With a TR monitor, the beam profile of as low as 15 MeV electrons can clearly be seen.

The current of the beam through SL5 was 200 mA. This value indicates that the emittance is estimated to be larger than in the specification by a factor of 2.1.

The performance of the linac system is summarized in table I . Performance satisfies the design specifications, except for the transverse emittance. The reason why the emittance is larger than expected is unclear. One possible reason is unsatisfactory adjustment.

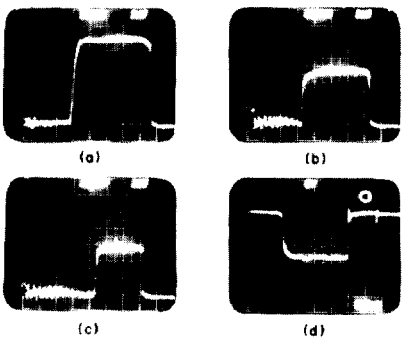

Fig. 3 Beam current waveforms.
vertical axis : 100 mA/div.
horizontal axis : 1 μsec/div. [(a), (b), (c)]
0.5 μsec/div. [(d)]
(a) at the point just after the electron gun. (CM1)
(b) at the exit of the accelerating cavities. (CM2)
(c) at the exit of the ECS. (CM3)
(d) at the exit of the energy analyzer. (FCM3)
energy aperture is 1%.

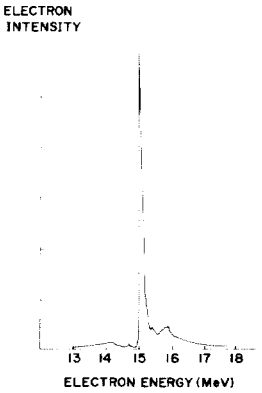

Fig. 4 Electron beam energy spectrum.

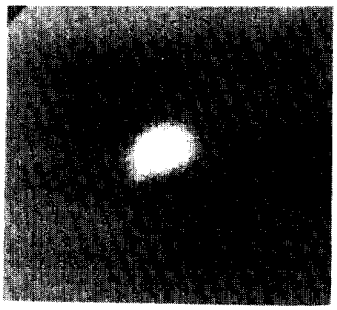

Fig. 5 Beam profile with the TR monitor (TR2) at the exit of the ECS.

References

[1] A. Heuberger, "X-ray Lithography," Microcircuit Engineering, vol. 3, pp.535-556, 1985.
[2] S. Mandai, Y. Hoshi and Y. Kohno, "Development of Compact Synchrotron Light Source for X-Ray Lithography," presented at The 3rd Int. Conf. on Synchrotron Radiation Instrumentation, Tsukuba, Japan, Aug. 29-Sept. 2, 1988.
[3] H. Yamada and SHI accelerator research group, "Compact Superconducting SR Light Source - AURORA," ibid.
[4] M. Q. Barton, B. Craft and G. P. Williams ed., "Report of the Second Workshop on Synchrotron Radiation Sources for X-ray Lithography," BNL-38789, 1986.
[5] A. Shibayama, T. Kitayama, T. Hayasaka, S. Ido, Y. Uno, T. Hosokawa, J. Nakata, K. Nishimura and M. Nakajima, "NTT Accelerating Storage Ring," presented at The 3rd Int. Conf. on Synchrotron Radiation Instrumentation, Tsukuba, Japan, Aug. 29-Sept. 2, 1988.
[6] T. Hosokawa, T. Kitayama, T. Hayasaka, S. Ido, Y. Uno, A. Shibayama, J. Nakata, K. Nishimura and M. Nakajima, "NTT Superconducting Storage Ring - Super-ALIS," ibid.
[7] Y. Takeuchi, H. Fujioka and K. Ura, "Invariants of Paraxial Trajectories in RF Electromagnetic Fields," Trans. IECE Japan, vol. 56-B, pp.551-558, Dec. 1973.